Expanded View Figures

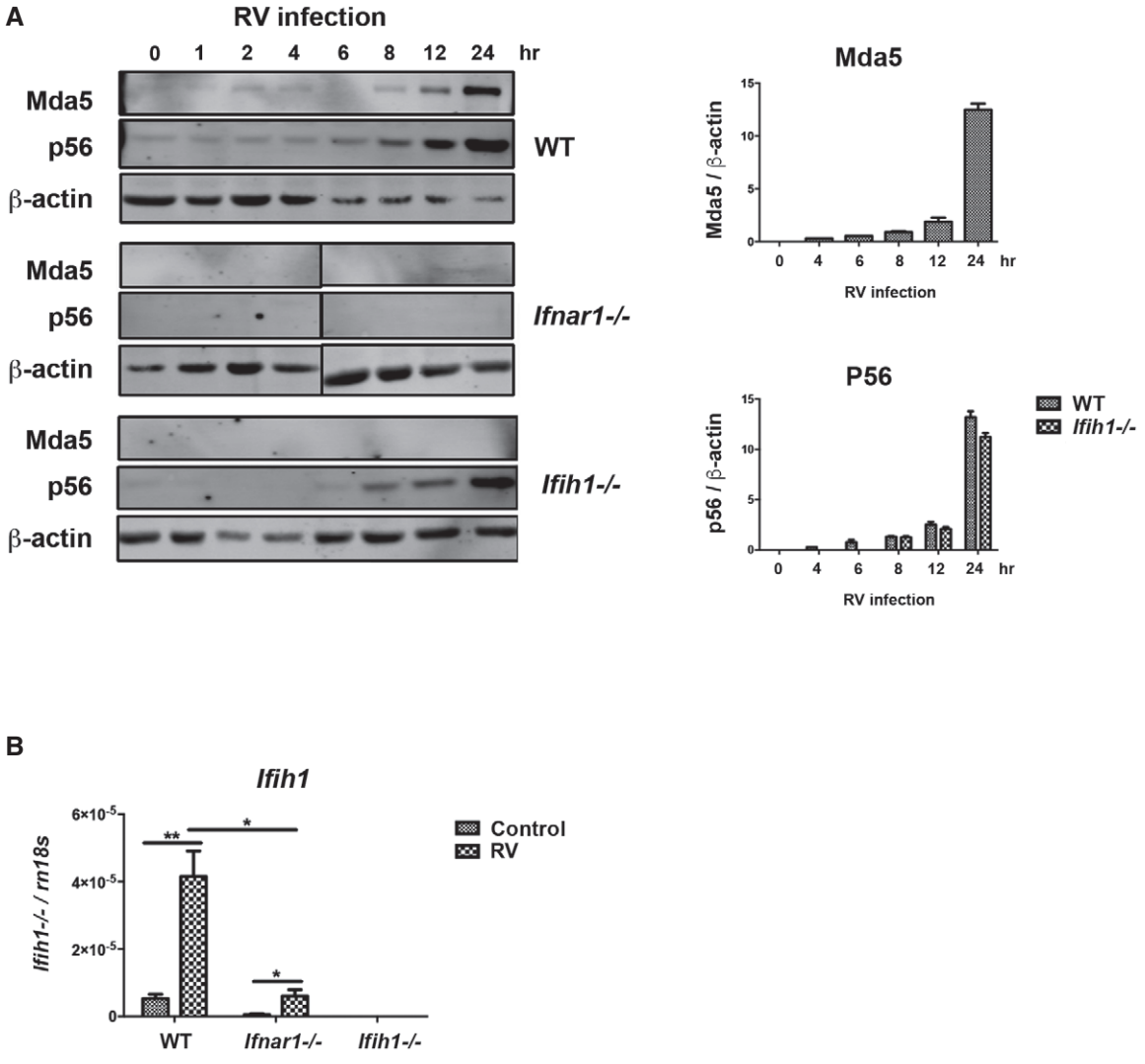

Figure EV1. Mda5 (*Ifih1*) and P56 induction in response to RV (related to Fig 2B–D).

A Detection (on left) and quantitation (on right) of Mda5 and P56 induction relative to β-actin in WT, *Ifnar1*$^{-/-}$, and *Ifih1*$^{-/-}$ MEFs infected with RV for the indicated times by immunoblot.

B Quantitation of the induction of the *Ifih1* mRNA in WT, *Ifnar1*$^{-/-}$, and *Ifih1*$^{-/-}$ MEFs 6 h post-infection with RV by qRT–PCR.

Data information: The data are shown as mean ± SEM. Student's *t*-test was used to calculate the *P*-values ($n = 3$). *$P \leq 0.05$, **$P \leq 0.01$.

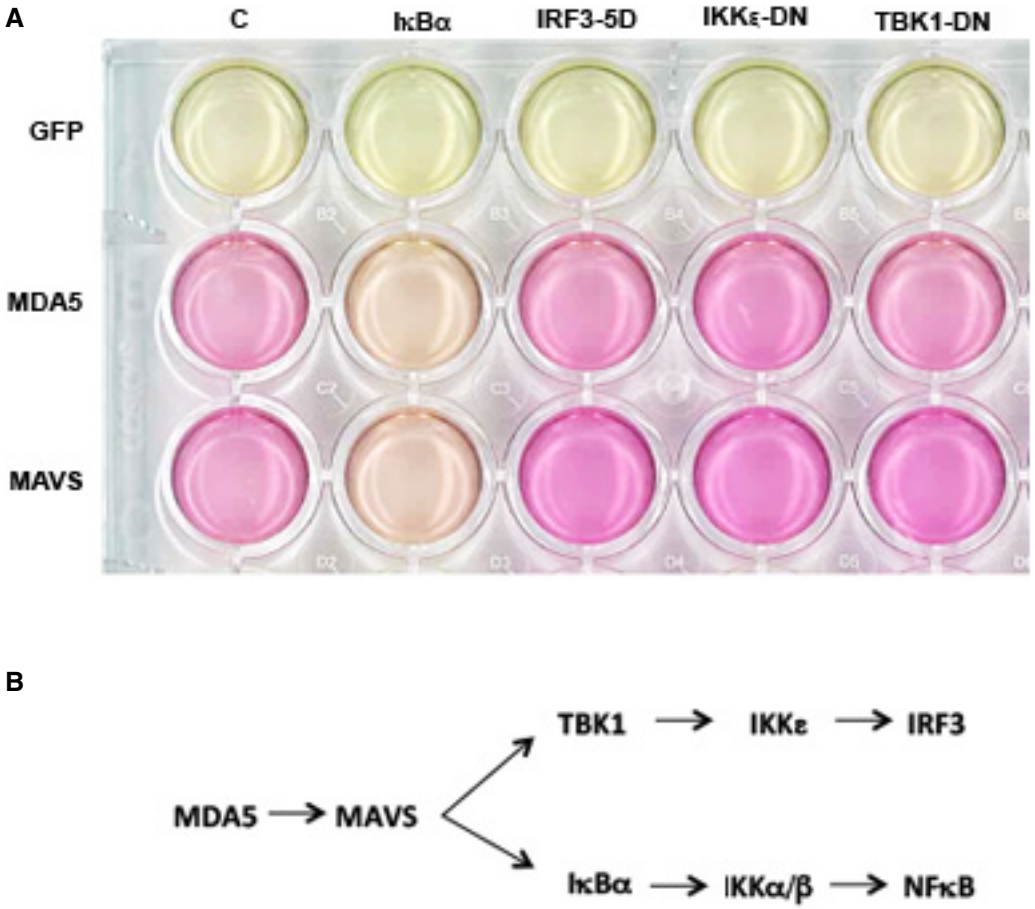

Figure EV2. MDA5-induced cell death in HEK293 cells is NFκB dependent (related to Fig 3F).

A Relative cell survival assessed by the pH-dependent color change of culture medium supporting HEK293 cells transfected with GFP, MDA5 or MAVS expression constructs, and a control backbone vector (C) or dominant-negative constructs of TANK-binding kinase 1 (TBK1-DN), IKK-related kinase ε (IKKε-DN), a constitutively active IRF3 construct (IRF3-5D), or the NFκB inhibitor, IκBα, after 90 h of culture.

B A schematic of MDA5-dependent cell signaling in the cell.

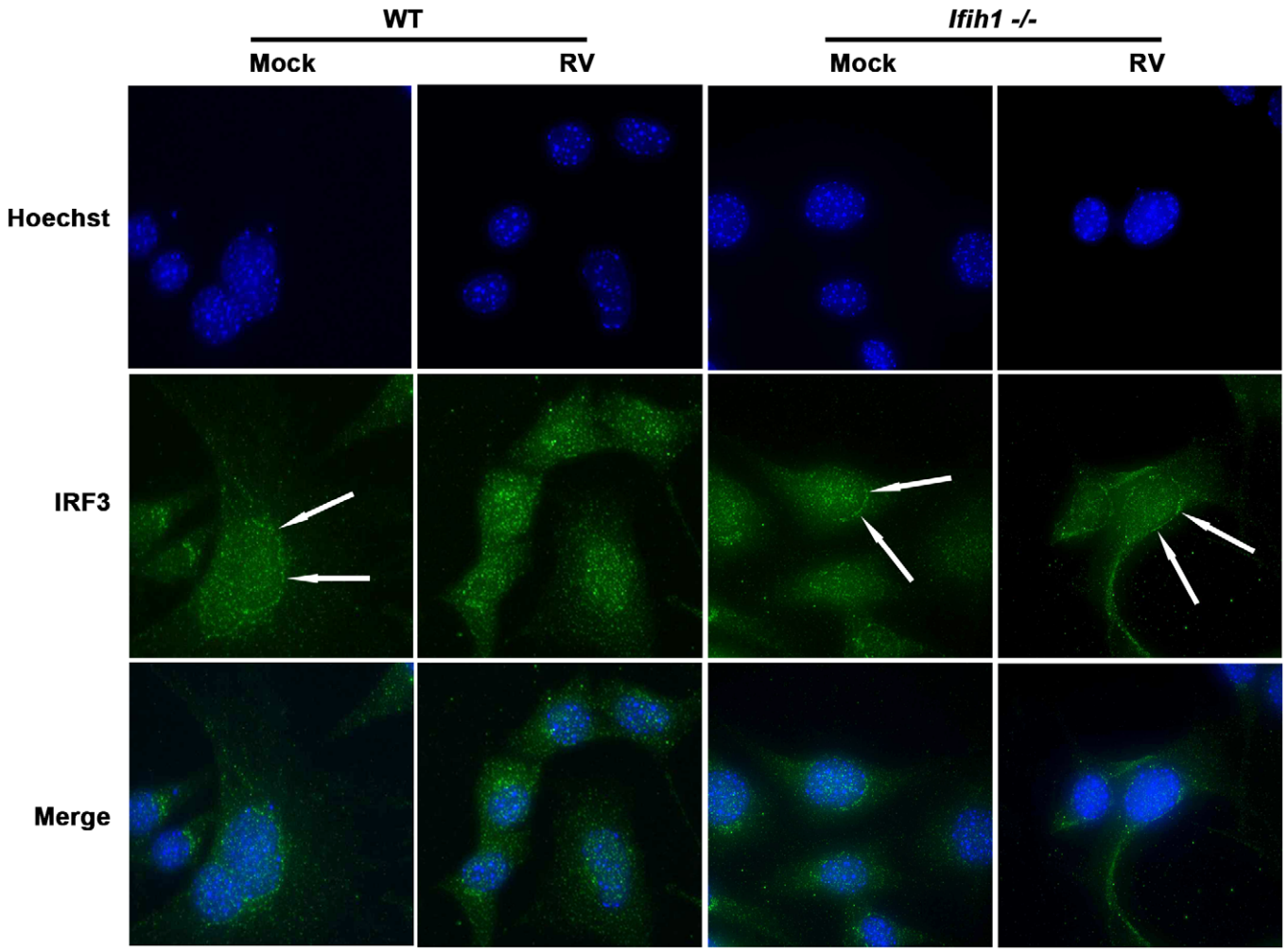

Figure EV3. Mda5-induced nuclear translocation of IRF3 in MEFs infected with RV (related to Fig 4).

Micrographs showing the cellular distribution of IRF3 (green) in WT and *Ifih1*$^{-/-}$ MEFs detected with an anti-IRF3 antibody 4 h after infection with RV. Arrows indicate the more intense cytosolic, perinuclear enrichment of IRF3 in the WT and *Ifih1*$^{-/-}$ cells before infection. This fluorescence pattern changes to a relatively more intense nuclear (blue) staining of IRF3 in RV-infected WT cells but not infected *Ifih1*$^{-/-}$ cells. The nucleus is visualized with the Hoechst DNA stain.

Figure EV4. Visualization of MDA5 expression and associations (related to Fig 7A–C).

A, B Micrographs showing GFP fluorescence in HEK293 cells transfected with the indicated LV-MDA5-GFP variants after 48 (A) and 56 h (B), showing that the cytosolic expressed fusion protein coalesces to a perinuclear signal.

C, D Micrographs showing Venus fluorescence in cells co-transfected with split-Venus constructs separately fused to the indicated MDA5 variants and either (C) MDA5 to detect homotropic interactions or (D) MAVS to detect hetero-oligomerization.

E A quantitation of the extent of the association of protein complexes with the mitochondria assessed by measuring the co-localization of Venus fluorescence with the signal from the MitoTracker stain as regions of interest (ROI). The data are shown as mean ± SD. Student's *t*-test was used to calculate the *P*-values from six measures for each protein pair at each time point. NS = $P > 0.05$, *$P \leq 0.05$, **$P \leq 0.01$, ***$P \leq 0.001$, ****$P \leq 0.0001$.

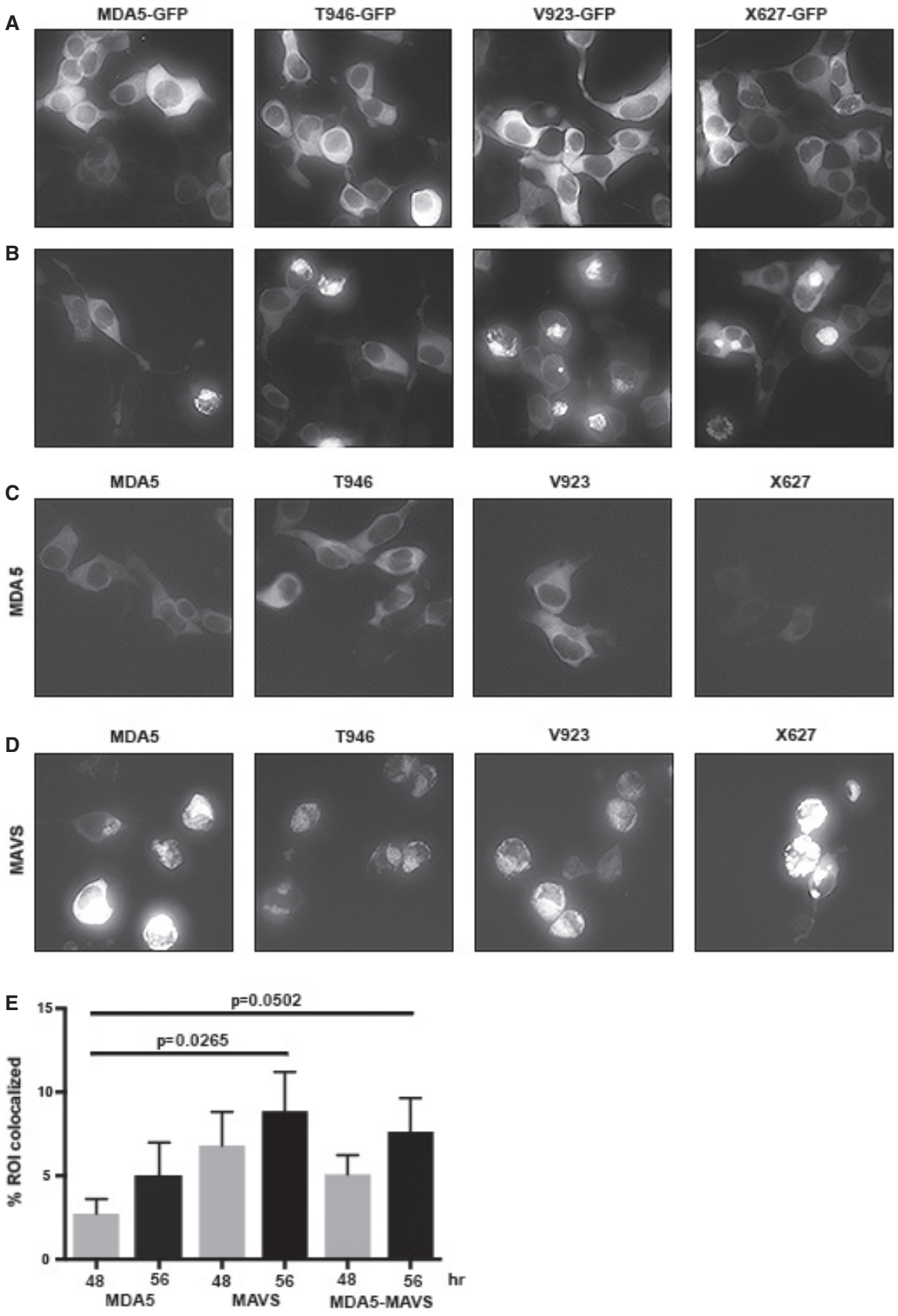

Figure EV4.

Figure EV5. Transient transfection assays with MDA5 lentiviral constructs (related to Fig 7D–G).

A, B Immunoblots detecting the induction of P56 to demonstrate the responsiveness of (A) HEK293 compared to (B) HEK293T (at top) and HeLa (at bottom) cells expressing MDA5 (*Ifih1*), RIG-I, or MAVS when treated with FuGENE:pIC to activate the RLRs. β-Actin is used as a loading control.

C FACS plots of HEK293 cells expressing LV-GFP or the indicated LV-MDA5-GFP variants stained with annexin V and 7-AAD. The data represent cellular viability in both transfected (GFP^+) and non-transfected cells (GFP^-). The GFP-, annexin V-, and 7-AAD-positive cells are graphed in Fig 7G.

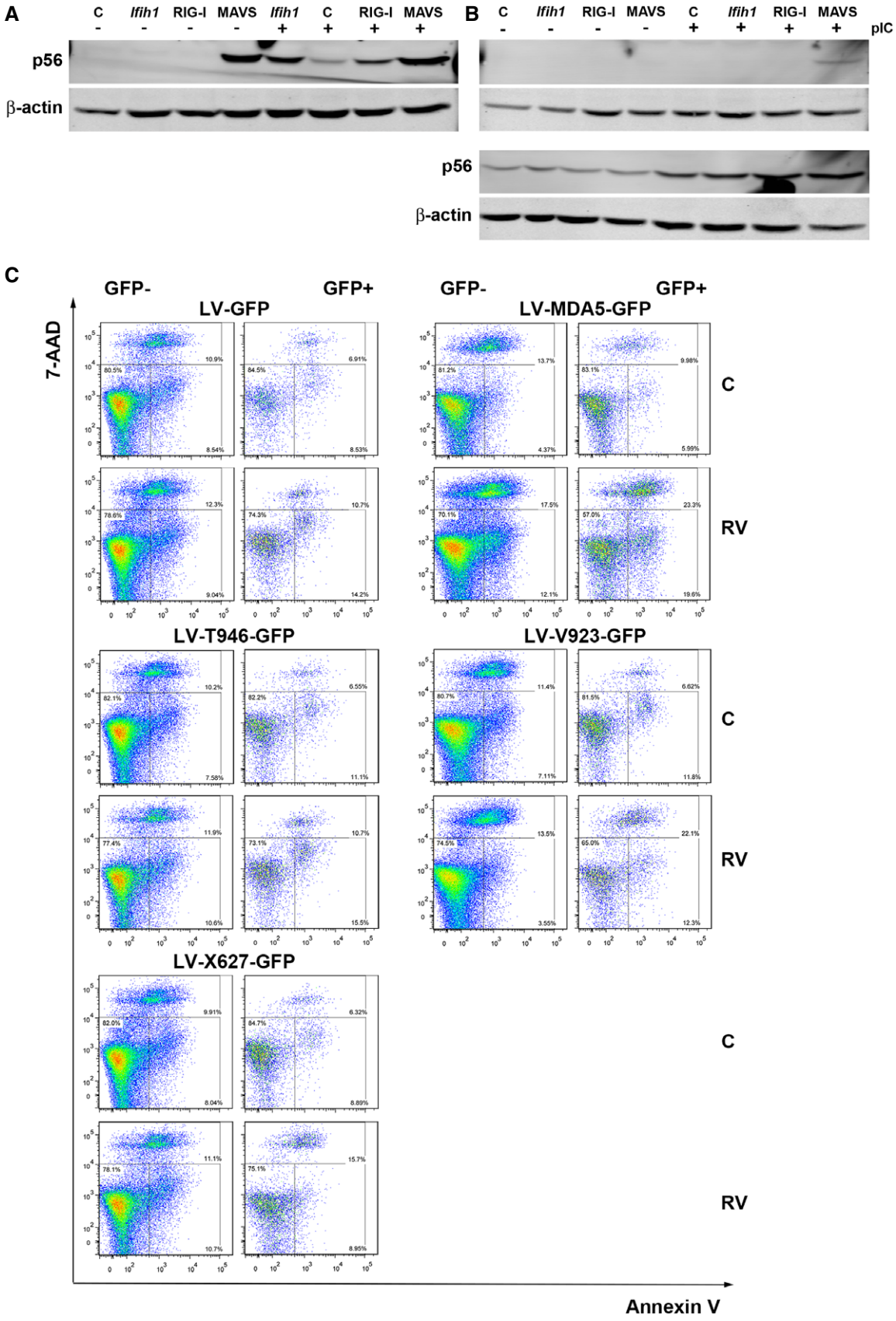

Figure EV5.

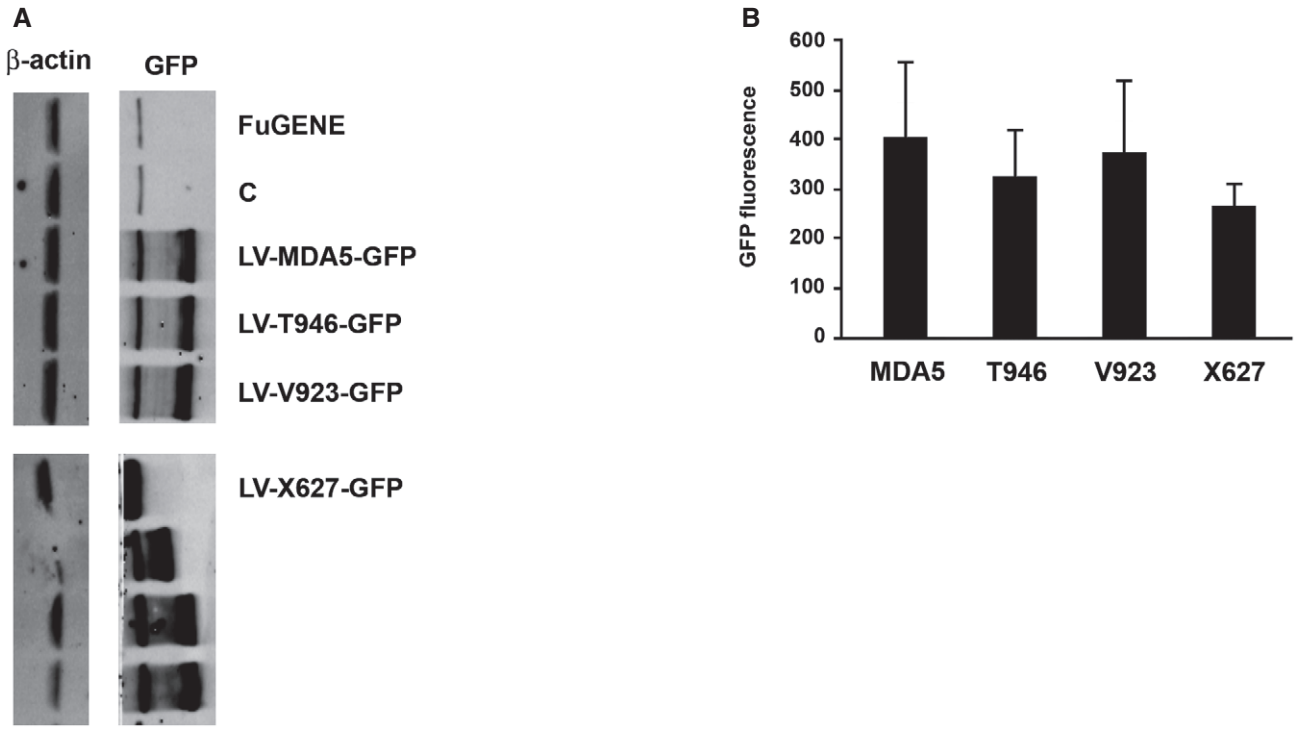

Figure EV6. MDA5-induced cell death (related to Fig 7H and I).

A Immunoblot detection of the expression of the indicated LV-MDA5-GFP constructs in HEK293 cells using an anti-GFP antibody. Unmarked lanes are mutant MDA5 constructs that were used as additional controls in the study that are not described in the text.

B A graph showing the relative GFP fluorescence produced in HEK293 cells transfected with the indicated LV-MDA5-GFP constructs. The data is shown as mean ± the SD ($n = 3$).